Spontaneous layering and power-law order in the three-dimensional fully packed hard-plate lattice gas

Geet Rakala,[1,*] Dipanjan Mandal,[2,†] Soham Biswas,[3] Kedar Damle,[4,‡] Deepak Dhar,[5,§] and R. Rajesh[6,7,‖]

[1]*Okinawa Institute of Science and Technology, 1919-1 Tancha, Onna-son, Kunigami-gun, Okinawa-ken, Japan*
[2]*Department of Physics, University of Warwick, Coventry CV4 7AL, United Kingdom*
[3]*Departamento de Fisica, Universidad de Guadalajara, Guadalajara, Jalisco, Mexico*
[4]*Department of Theoretical Physics, Tata Institute of Fundamental Research, Mumbai 400005, India*
[5]*Indian Institute of Science Education and Research, Dr. Homi Bhabha Road, Pashan, Pune 411008, India*
[6]*The Institute of Mathematical Sciences, C.I.T. Campus, Taramani, Chennai 600113, India*
[7]*Homi Bhabha National Institute, Training School Complex, Anushakti Nagar, Mumbai 400094, India*

(Received 9 February 2022; accepted 7 June 2023; published 26 June 2023)

We obtain the phase diagram of fully packed hard plates on the cubic lattice. Each plate covers an elementary plaquette of the cubic lattice and occupies its four vertices, with each vertex of the cubic lattice occupied by exactly one such plate. We consider the general case with fugacities s_μ for "μ plates," whose normal is the μ direction ($\mu = x, y, z$). At and close to the isotropic point, we find, consistent with previous work, a phase with long-range sublattice order. When two of the fugacities s_{μ_1} and s_{μ_2} are comparable, and the third fugacity s_{μ_3} is much smaller, we find a spontaneously layered phase. In this phase, the system breaks up into disjoint slabs of width two stacked along the μ_3 axis. μ_1 and μ_2 plates are preferentially contained entirely within these slabs, while plates straddling two successive slabs have a lower density. This corresponds to a twofold breaking of translation symmetry along the μ_3 axis. In the opposite limit, with $\mu_3 \gg \mu_1 \sim \mu_2$, we find a phase with long-range columnar order, corresponding to simultaneous twofold symmetry breaking of lattice translation symmetry in directions μ_1 and μ_2. The spontaneously layered phases display critical behavior, with power-law decay of correlations in the μ_1 and μ_2 directions when the slabs are stacked in the μ_3 direction, and represent examples of "floating phases" discussed earlier in the context of coupled Luttinger liquids and quasi-two-dimensional classical systems. We ascribe this remarkable behavior to the constrained motion of defects in this phase, and we sketch a coarse-grained effective field theoretical understanding of the stability of power-law order in this unusual three-dimensional floating phase.

DOI: 10.1103/PhysRevE.107.064137

I. INTRODUCTION

Fully packed dimer models have been studied for several decades. On the one hand, they provide fascinating examples of entropically driven ordering, closely analogous to Villain's "order-by-disorder" phenomena in frustrated magnets [1]. On the other hand, on bipartite lattices, they also host highly correlated liquid phases [2]. These "Coulomb phases" admit a natural description in terms of a field theory for polarization fields. This is a coarse-grained version of a lattice-level description in which each fully packed dimer configuration of the bipartite lattice is mapped to a divergence-free vector field on links of the lattice [3,4]. In the two-dimensional cases of square and honeycomb lattices, this effective field theory correctly describes [5–9] the power-law columnar-ordered state of the fully packed dimer model on these lattices. In the three-dimensional cases of the cubic and diamond lattice, this correctly predicts that the fully packed dimer model on these bipartite lattice displays a Coulomb liquid phase with dipolar power-law correlations between the dimers [10].

Here we study a fully packed lattice gas of plates. Each plate covers an elementary plaquette of the cubic lattice and occupies its four vertices. At full-packing, each site of the lattice is occupied by exactly one plate. The key question then is whether such a lattice gas displays a correlated liquid phase that could be understood in coarse-grained field-theoretical language in terms of tensor-valued analogs of the fluctuating polarization fields that describe the behavior of the fully packed dimer model. This is a natural speculation since one may view each plate as a pair of parallel dimers on the corresponding plaquette, which translates to two antiparallel dipoles that form a quadrupole. Such a liquid phase would control properties of the corresponding resonating plaquette liquid states of SU(4) magnets [11] in much the same way as the Coulomb liquid phase of the interacting two-dimensional dimer model provides a description of energy correlations of resonating short-range valence bond wave functions [12,13] of SU(N) magnets [14]. Motivated perhaps by this natural line of thought, previous work [15] used Monte Carlo simulations

*geet.rakala@oist.jp
†dipanjan.mandal@warwick.ac.uk
‡kedar@theory.tifr.res.in
§deepak@iiserpune.ac.in
‖rrajesh@imsc.res.in

to study fully packed hard plates on the cubic lattice, with equal fugacities for plates of all orientations. It was found however that fully packed hard plates on the cubic lattice exhibit long-range sublattice order [15], instead of this kind of correlated liquid behavior.

Here, we explore the rich phase diagram of this fully packed lattice gas of hard plates in the general case with fugacities s_μ for "μ plates," i.e., with normal in direction μ ($\mu = x, y, z$). At and close to the isotropic point ($s_x = s_y = s_z$), we find a phase with long-range sublattice order, i.e., with twofold (Z_2) symmetry breaking of lattice translation symmetry in all three directions, consistent with the previous results alluded to earlier. When two of the fugacities s_{μ_1} and s_{μ_2} are comparable, and the third fugacity s_{μ_3} is much smaller, we find a spontaneously layered phase. In this phase, the system breaks up into disjoint slabs of width two stacked along the μ_3 axis. μ_1 and μ_2 plates are preferentially contained entirely within these slabs, while plates straddling two successive slabs have a lower density. This corresponds to a twofold symmetry breaking of translation symmetry along the μ_3 axis, leading to "occupied slabs" stacked in the layering direction with a separation of one lattice spacing. In the opposite limit, with $\mu_3 \gg \mu_1 \sim \mu_2$, we find a phase with long-range columnar order, corresponding to simultaneous Z_2 symmetry breaking of lattice translation symmetry in directions μ_1 and μ_2. The spontaneously layered phases display critical behavior, with power-law decay of correlations in the μ_1 and μ_2 directions when the slabs are stacked in the μ_3 direction. The spontaneously layered phase represents an example of a "floating phase," of the type discussed earlier in the context of coupled Luttinger liquids and quasi-two-dimensional classical systems [16,17].

To understand the stability of this unusual phase, we identify the key ingredients of an effective field theory for this phase. This builds on a coarse-grained description used earlier for mixtures of dimers and hard squares on the two-dimensional square lattice [18]. The basic idea is as follows: Consider the limit of a perfectly layered phase, with layering along (say) the z direction. When the layering is perfect, x and y plates are entirely contained within disjoint slabs of width two along the z axis, with no x or y plates straddling two successive slabs. Viewed along the z axis, each occupied slab looks like a system of dimers and hard squares on a two-dimensional square lattice. Interslab plates that straddle two successive slabs give rise to defects. We argue that these interslab plates are bound in pairs in the layered phase.

We develop an effective field theory description in which such pairs of interslab plates correspond to quadrupolar couplings between two successive two-dimensional systems. The quadrupolar nature of these couplings render them irrelevant at the critical fixed point that describes each power-law-ordered two-dimensional layer, leading to a stable floating phase. Thus, this perspective leads us to identify the binding of dipolar defects into quadrupoles as being the key to the stability of this floating layered phase. Microscopically, this arises from the full-packing condition, which leads to constraints on existence and motion of interslab defects in this layered phase.

The mechanism that stabililizes this phase is thus closely related to the physics of fractonic phases that have attracted a great deal of attention recently [19–22]. These considerations also suggests that this lattice gas of hard plates may have interesting behaviors in the presence of a small density of vacancies, due to restrictions on the configuration and motion of vacancies. The effect of vacancies has been studied in a parallel work [23].

The rest of this paper is organized as follows: In Sec. II we first define the model and the order parameters used to identify its phases, and provide an overview of the phase diagram deduced from the results of our Monte Carlo simulations. Sec. III is devoted to a summary of our Monte Carlo simulation method. In Sec. IV we present the computational evidence for the phase diagram described in Sec. II. Sec. V is devoted to a closer look at the unusual structure of correlations exhibited by the layered phase, and a sketch of a coarse-grained field-theoretical description of this phase. Finally, we conclude in Sec. VI with a brief discussion of some questions that may be interesting to address in follow-up work.

II. MODEL, PHASE DIAGRAM, AND ORDER PARAMETERS

As already outlined in Sec. I, we study a fully packed lattice gas of hard plates that each occupy all four sites of an elementary plaquette of the cubic lattice. We consider the general case with fugacities s_μ for μ plates, i.e., with normal in direction μ ($\mu = x, y, z$). With periodic boundary conditions, the L^3 sites of an $L \times L \times L$ cubic lattice, where L is even, are covered by $L^3/4$ hard plates in every such fully packed configuration. We adopt the convention that the plate fugacities obey the constraint:

$$s_x + s_y + s_z = 3. \tag{1}$$

The partition function of the system is now given as

$$Z = \sum_C s_x^{n_x} s_y^{n_y} s_z^{n_z}, \tag{2}$$

where the sum is over all the fully packed configurations of such a cubic lattice and n_x, n_y, and n_z are the total number of x, y, and z plates in the configuration C. An illustrative example of a configuration of the $L = 4$ cubic lattice with periodic boundary conditions is shown in Fig. 1.

The parameter space of this fully packed lattice gas is conveniently represented by an equilateral *fugacity triangle*, with the three vertices corresponding to $s_x = 3$, $s_y = 3$, and $s_z = 3$, respectively, as shown in Fig. 2. The sides of this triangle then correspond to the $s_x = 0$, $s_y = 0$, and $s_z = 0$ lines. The centroid of this triangle represents the isotropic point where $s_x = s_y = s_z = 1$. In our computational work, we have focused on obtaining results along the two cuts shown in Fig. 2. With the parameter e defined as $e \equiv s_x - s_y$, these two cuts through the phase diagram correspond to $e = 0$ and $e = 0.3$ (dashed and dotted vertical lines in Fig. 2). Using results from simulations along these two cuts, we have been able to map out the overall structure of the phase diagram in this fugacity triangle. This is discussed in more detail below after introducing the various observables that allow us to characterize the different phases.

In our computational work, it is convenient to adopt a convention whereby each plate is assigned to a unique lattice site i as follows: Any plate occupies four lattice sites. Each

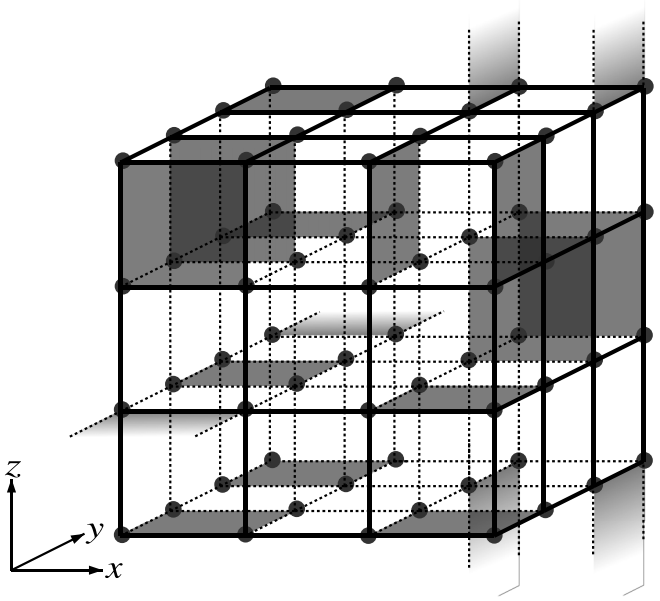

FIG. 1. A configuration of hard plates at full packing on the $L = 4$ cubic lattice with periodic boundary conditions. Each plate occupies exactly four sites of an elementary square plaquette of the cubic lattice, and each site of the cubic lattice is occupied by exactly one such plate in the fully packed case.

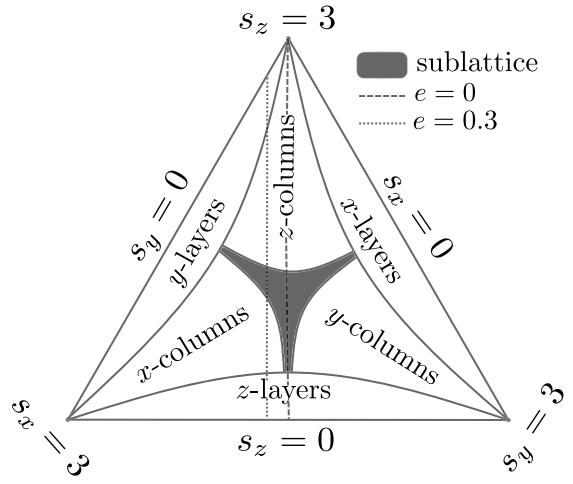

FIG. 2. The fugacity triangle shown in the figure represents the parameter space of the fully packed hard square lattice gas. Note that the fugacities s_μ ($\mu = x, y, z$) satisfy $s_x + s_y + s_z = 3$ in our convention. Then, the corners of the triangle correspond to the points $s_x = 3$, $s_y = 3$, and $s_z = 3$, respectively, while the sides correspond to the lines $s_x = 0$, $s_y = 0$, and $s_z = 0$, respectively. The dashed and dotted vertical lines correspond to $s_x - s_y = 0$ and 0.3, respectively. They represent the cuts along which our most detailed numerical results have been obtained. There are three kinds of phases: A sublattice-ordered phase, with lattice translation symmetry broken in all three Cartesian directions, layered phases with lattice translation symmetry broken only along one Cartesian direction, and columnar-ordered phases with lattice translation symmetry broken along two of the three Cartesian directions.

plate in the bulk is assigned to the site i (chosen from these four sites) that has the minimum value of all three Cartesian coordinates $x(i)$, $y(i)$, and $z(i)$. For plates that wrap around, this rule is modified in the obvious way for the Cartesian coordinate(s) along which periodicity is being imposed. In the fully packed limit, this implies that one-fourth of the lattice sites are assigned to plates and the rest are occupied by plates assigned to an adjacent lattice site.

Using this convention, we define two kinds of occupation variables on each site of the lattice: the single plate occupation $\phi_\mu(i)$, which takes a value 1 if a μ plate is assigned to the site i and 0 otherwise, and the double plate occupation number defined as $\phi_{\mu\mu}(i) = \phi_\mu(i)\phi_\mu(i + \hat{\mu})$, where $\hat{\mu}$ is the unit translation along the positive μ axis (the definition of $\hat{\mu}$ also incorporates periodic boundary conditions in all three directions).

We mainly use three different order parameters to quantitatively probe the nature of the various phases. These are the layering order parameter vector $\vec{\mathcal{L}}$, the columnar order parameter vector $\vec{\mathcal{C}}$ and the scalar sublattice order parameter ω. We now define each of these.

The layering vectors $\mathcal{L}_\mu$ and $\mathcal{L}_{\mu\mu}$ are defined to measure translation symmetry breaking along direction μ. For $\mathcal{L}_\mu$, we have

$$\mathcal{L}_x = \frac{1}{L^3}\sum_i l_x(i),$$
$$l_x(i) = (-1)^{x(i)}[\phi_x(i) + \phi_y(i) + \phi_z(i)], \tag{3}$$

and similarly for $\mathcal{L}_y$ and $\mathcal{L}_z$. The layering vector $\mathcal{L}_{\mu\mu}$ is defined in an entirely analogous manner, with all ϕ_γ in the above replaced by $\phi_{\gamma\gamma}$. The corresponding definition of the columnar vectors $\mathcal{C}_\mu$ and $\mathcal{C}_{\mu\mu}$ is chosen to ensure that these vector order parameters are sensitive to translation symmetry breaking in the two Cartesian directions perpendicular to μ. Thus, we define

$$\mathcal{C}_x = \frac{1}{L^3}\sum_i c_x(i),$$
$$c_x = (-1)^{y(i)+z(i)}[\phi_x(i) + \phi_y(i) + \phi_z(i)], \tag{4}$$

and cyclically for the other components $\mathcal{C}_y$ and $\mathcal{C}_z$. The layering vector $\mathcal{C}_{\mu\mu}$ is again defined as above, but with all ϕ_γ replaced by $\phi_{\gamma\gamma}$.

In addition, we define the scalar sublattice order parameter ω to measure the simultaneous breaking of translation invariance along all three directions:

$$\omega = 27\mathcal{L}_x\mathcal{L}_y\mathcal{L}_z, \tag{5}$$

where the factor of 27 is simply a convenient convention. This product probes the presence of sublattice order. It differs from the other order parameters defined here in an important way: Unlike the layering and columnar vectors, it is not defined as a sum over a corresponding local density field on the lattice. Instead, it is simply the product of three components of the layering vector $\mathcal{L}_\mu$. This has implications for its finite-size scaling properties, which will be discussed in Sec. IV.

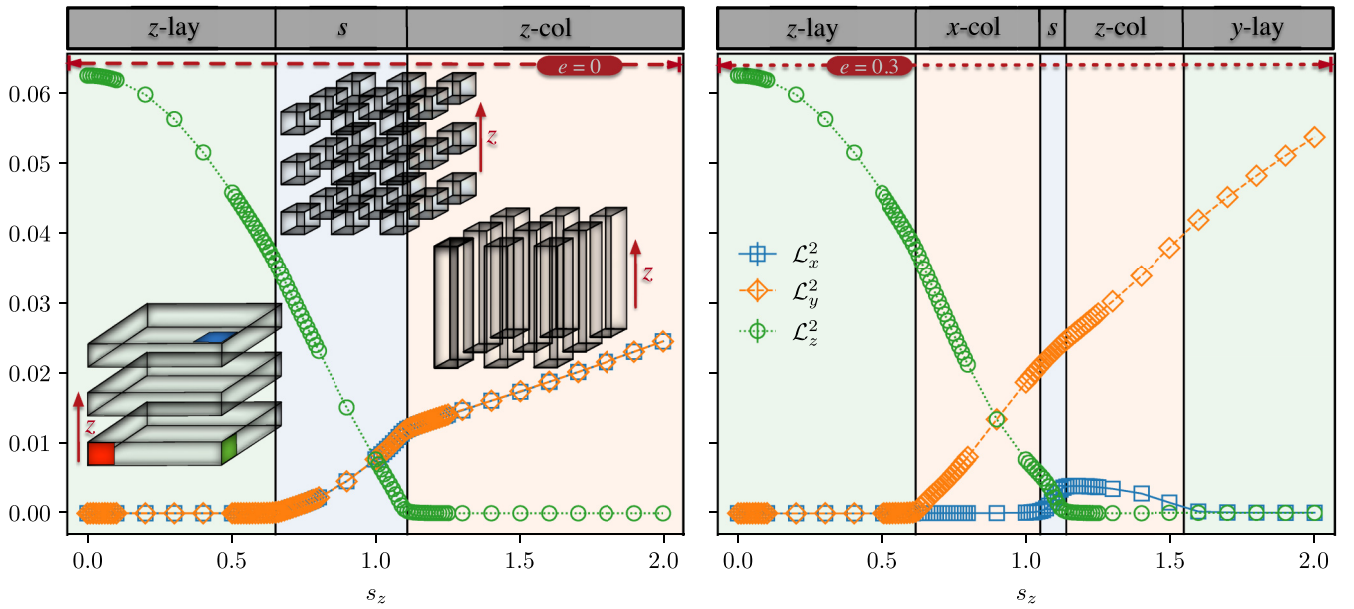

FIG. 3. The behavior of the three Cartesian components of the layering vector $\vec{\mathcal{L}}$ [defined in Eq. (3)] as a function of z plate fugacity s_z at $L = 72$ provides a convenient signature of the different ordered phases in various parts of the phase diagram. The left (right) figure corresponds to the $e = 0$ ($e = 0.3$) cut shown as a dashed (dotted) line in Fig. 2. To interpret these $L = 72$ results, it is useful to note the theoretical expectations outlined in Sec. II. Guided by these theoretical considerations, one can recognize at a glance the presence of various ordered states in different parts of the phase diagram; the existence of these ordered states can then be verified by more detailed analysis of the L dependence of various observables, as outlined in Sec. II (and discussed in detail in subsequent sections). Notation: z-col refers to columnar ordering along z, while z-lay refers to layering order along z, and likewise for other directions. s refers to sublattice ordering. Shown in the insets are schematic depictions of the system in the z-layered phase, the sublattice-ordered phase, and the z columnar-ordered phase. In this schematic depiction, the hard plates are free to rearrange (while respecting the full-packing constraint) only within the gray regions. Representative x, y, and z plates have been shown in red, green, and blue, respectively.

Before proceeding further, we comment on this unusual choice for the sublattice order parameter. A more natural and conventional choice would have been to use the double-plate occupation variables $\phi_{\mu\mu}(i)$ to define a sublattice order parameter obtained as a sum of a local order parameter density as follows:

$$Q = \frac{1}{L^3}\sum_i q(i),$$
$$q = (-1)^{x(i)+y(i)+z(i)}[\phi_{xx}(i) + \phi_{yy}(i) + \phi_{zz}(i)]. \qquad (6)$$

Indeed, the naturalness of this choice of Q as a probe for sublattice symmetry breaking was our original rationale for introducing the double-plate occupation variables and corresponding versions of $\mathcal{L}$ and $\mathcal{C}$ in the first place. However, it turns out that there is an unexpected difficulty with using Q to probe sublattice symmetry breaking: Q appears to tend to zero in the thermodynamic limit even in the sublattice-ordered phase. Although this is an interesting feature of the sublattice-ordered phase in its own right, it is peripheral to the main focus of our present study. We therefore use the sublattice order parameter ω in what follows, and only return to the unexpected behavior of Q in Sec. VI at the end of this paper.

In a layered phase with broken translation symmetry along exactly one Cartesian direction, only one component of the layering vector (corresponding to the layering direction) is expected to tend to a nonzero value in the thermodynamic limit. In the sublattice-ordered phase with broken translation symmetry in all three Cartesian directions, all three components of the layering vector are expected to tend to a nonzero value in the thermodynamic limit, and the three components are expected to be equal in magnitude at the isotropic point ($e = 0$ and $s_z = 1$). In a columnar-ordered phase

TABLE I. Table showing various order parameters (OP) and the long-range-ordered phases probed by these order parameters. Each row of the table corresponds to an order parameter, and each column corresponds to a long-range-ordered phase. Each entry in the table is a binary label "1" ("0") that indicates a nonzero (vanishing) thermodynamic limit for the order parameter that labels the row of that entry in the phase that labels its column. x-col refers to a columnar-ordered phase with columns along x, while x-lay refers to a layered phase with layering along x, and likewise for other directions. The order parameters constructed using the alternate double-plate definitions behave in the same manner. See Sec. II for details.

OP	x-col	y-col	z-col	x-lay	y-lay	z-lay	Sublattice
$\mathcal{L}_x^2$	0	1	1	1	0	0	1
$\mathcal{L}_y^2$	1	0	1	0	1	0	1
$\mathcal{L}_z^2$	1	1	0	0	0	1	1
$\mathcal{C}_x^2$	1	0	0	0	0	0	1
$\mathcal{C}_y^2$	0	1	0	0	0	0	1
$\mathcal{C}_z^2$	0	0	1	0	0	0	1
ω^2	0	0	0	0	0	0	1

with translation symmetry breaking along two directions, two components of the layering vector, corresponding to the two directions perpendicular to the orientation of columns of the columnar phase, are expected to tend to a nonzero value in the thermodynamic limit. Similar considerations hold for the columnar vector.

We summarize the various order parameters and the ordering patterns they probe in Table I. The layering and columnar ordering vectors defined using double plate occupation variables have been observed to behave exactly as their single plate counterparts and have therefore been omitted in Table I.

In the same spirit, a convenient way to summarize our findings along the two cuts shown in Fig. 2 is to plot the behavior of the three components of the layering vector $\vec{\mathcal{L}}$ along these cuts. This is shown in Fig. 3. The accompanying insets of Fig. 3 provide a schematic depiction of the nature of symmetry breaking in the different ordered states detected in our simulations along these two representative scans. Supplementing the information depicted in Fig. 3 with results for the L dependence of all the order parameters and the corresponding Binder coefficients (discussed separately in Sec. IV), and using the threefold symmetry of the phase diagram, allows us to deduce the structure of the phase diagram in the whole equilateral triangle, as shown in Fig. 2.

As shown in Fig. 2, we find a phase with long-range sublattice order at and close to the isotropic point, i.e., when all three fugacities are comparable to each other, and the corresponding densities are likewise comparable. This finding is consistent with a previous study of isotropic fully packed plates, which found in favor of a sublattice-ordered state [15]. Our study allows us to go beyond this and study the competition between this sublattice-ordered phase and the layered and columnar-ordered phases for general values of the fugacities.

Indeed, when two of the fugacities s_{μ_1} and s_{μ_2} are comparable, and the third fugacity s_{μ_3} is much smaller, we find a spontaneously layered phase with Z_2 symmetry breaking of lattice-translation symmetry in the μ_3 direction. In this phase, the system breaks up into disjoint slabs of thickness two, such that a majority of the μ_1 and μ_2 plates are fully within one of the slabs. In the opposite limit, with $\mu_3 \gg \mu_1 \sim \mu_2$, we find a phase with long-range columnar order, corresponding to simultaneous Z_2 symmetry breaking of lattice translation symmetry in directions μ_1 and μ_2.

III. COMPUTATIONAL METHODS

Our Monte Carlo simulations use a combination of local updates, supplemented by a cluster algorithm to improve the equilibration and reduce autocorrelation times. We use two types of local updates: a *ring* exchange move, and a *shift* exchange move.

A. Ring exchange

The ring exchange move, shown in Fig. 4, relies on the fact that all eight vertices of an elementary cube can be occupied by two plates that cover two opposite faces of the cube. There are three such "perfect covers" of any elementary cube. To implement the ring exchange move, we pick an elementary cube at random and if it is perfectly covered, we choose afresh a fully packed configuration for the cube with probabilities that satisfy detailed balance [24].

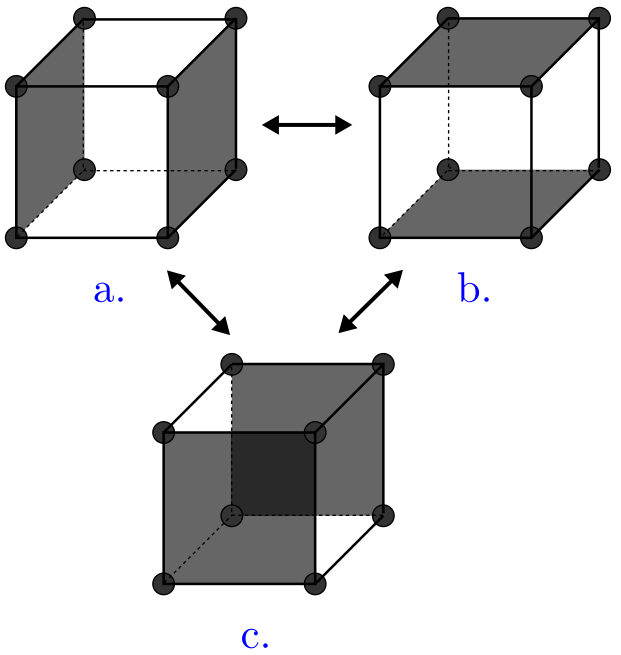

FIG. 4. All the possible local moves in a ring exchange move.

B. Shift exchange

The *shift* exchange starts by picking a random pair of adjacent elementary cubes sharing a face of the lattice with each other. Let the shared face have a normal in the μ direction. If one of the elementary cubes is perfectly covered by a pair of ν plates, where $\nu \neq \mu$, and the other elementary cube has its remaining four sites occupied by a μ plate, then the configurations of the two elementary cubes are interchanged (see Fig. 5). Since this does not change the orientation of the three plates involved, the shift exchange is implemented with probability 1, whenever the chosen pair of elementary cubes has an eligible configuration.

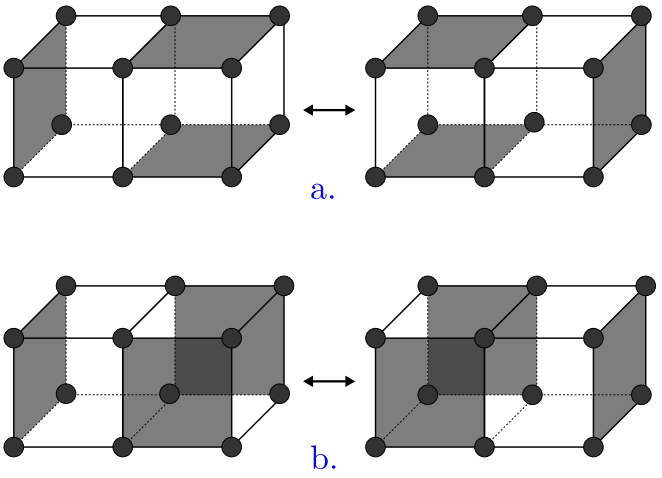

FIG. 5. All the possible local moves in a shift exchange.

To supplement these two updates and improve autocorrelation times of the Monte Carlo algorithm, particularly in the presence of periodic boundary conditions, one can use two kinds of nonlocal updates. The first uses a transfer matrix method to update an entire one dimensional tube, keeping the rest of the configuration fixed. This generalizes the approach used previously for simulations of a mixture of hard squares and dimers in two dimensions [18]. The other is a cluster algorithm that generalizes the pocket cluster algorithm [25] used previously to study fully packed dimer models.

Here, we show results obtained using the second approach to supplement local moves, i.e., using a generalization of the pocket cluster algorithm [25]. However, parallel work [23] that studies the effect of vacancies uses the transfer matrix update [18] since the presence of vacancies improves its performance. We note that the pocket cluster algorithm leads to slightly better error bars for various order parameters in the fully packed case.

In the cluster update scheme, we rely on the existence of $\mathcal{O}(L)$ different reflection symmetries of the system, each of which square to the identity operation. For this to be the case, periodic boundary conditions are essential. To begin, a reflection is specified by picking a randomly chosen reflection plane. Six kinds of reflection planes, each perpendicular to one of the three Cartesian directions and either containing sites of the lattice or bisecting bonds of the lattice, always define valid symmetry operations for general values of fugacities. Of these, we choose to use the $3L$ planes that contain sites of the lattice. In addition, one can consider reflections about "diagonal" reflection planes, specified by a normal that lies either in the xy plane and makes an angle of $\pm\pi/4$ with the x and y axis, or does the same in the yz or zx plane. These six kinds of additional reflections are all symmetries of the system only at the isotropic point when all the fugacities are equal. Elsewhere in the fugacity triangle, at most two of them are symmetries.

The cluster update begins by randomly choosing (with equal probability) one of the possible reflection symmetries of the system, say a reflection about the symmetry plane $\mathcal{S}$. In addition, a plate is chosen at random as the seed. Apart from the physical system, one constructs a "pocket lattice," which is empty to begin with. The seed plate is acted on by the reflection operation corresponding to the randomly chosen symmetry plane $\mathcal{S}$. This can change its location, and, possibly its orientation too. Thus transformed, the plate is moved to the pocket lattice and placed in its possibly new location (and possibly new orientation). Next, this transformed plate is moved back to the physical lattice so that it now occupies a transformed location with a transformed orientation in the physical lattice. As a result, it touches some other plates in the physical lattice. These other plates are now removed from the physical lattice, transformed according to the symmetry operation $\mathcal{S}$, and moved to the pocket lattice.

The rest of the update consists of repeating this process until the pocket lattice is empty. In other words, at each step, we take a plate from the pocket lattice, move it back to the physical lattice so that it occupies a transformed location with a transformed orientation, and then remove the plates it touches in the physical lattice, transform them, and move them to the pocket lattice. Once the pocket lattice is emptied at the end of this process, the physical lattice again has a fully packed configuration that does not violate any constraints. This new configuration can be accepted with probability one since the weight of the configuration has not changed in this process.

We simulate the system using a combination of these local and cluster updates. Each Monte Carlo step (MCS) involves L^3 ring exchanges, L^3 shift exchanges in the $\hat{x}$, $\hat{y}$, and $\hat{z}$ directions each, and a number of cluster updates, each involving a randomly chosen symmetry plane and a random seed plate (this number is chosen to ensure that a total of $\mathcal{O}(L^3)$ plates are involved in these cluster updates as a whole). The Monte Carlo routine was tested against exact enumeration on a $4 \times 4 \times 2$ periodic lattice with fully packed hard plates using Martin's backtracking algorithm [26].

At each set of fugacity parameters, simulations were carried out on lattices of size $L = 48, 60, 72, 96$, and 120. Some intralayer and interlayer observables (Figs. 7–9) have also been estimated at $L = 144$. Simulations at each set of parameter values usually involved at least 10 random initial seeds, a random initial configuration, a warmup of 2×10^5 MCS for each seed, followed by a run length of 2×10^6 MCS for each seed. The data shown in the zoomed-in plot of Binder ratios in Fig. 10 involved averaging over runs from 50 random initial seeds. Independent simulations at each set of parameter values were parallelized using GNU Parallel. After warmup, measurements were made at alternate MCS in each Monte Carlo run. 10^3 such measurements were binned to create one notionally independent measurement. Error bars were estimated by rebinning these notionally independent measurements in sets of 5, 50, and 100 and using the rebinned estimators to calculate three different estimates of the statistical error. The actual error bar assigned to each data point was taken to be the maximum of these three estimates.

IV. COMPUTATIONAL RESULTS

The overview presented in Fig. 3 shows the fugacity dependence of the different components of the layering order parameter at a fixed size $L = 72$ along two cuts through the fugacity triangle, and provides a direct graphic indication of the nature of the phases in different parts of the phase diagram.

To go beyond this and quantify the symmetry breaking and pin down the phase boundaries, we study the L dependence of various observables. For each order parameter $\mathcal{O}$ defined in Sec. II, we monitor the L dependence of $\langle \mathcal{O}^2 \rangle$ to determine whether the phase in question is characterized by the corresponding long-range ordering behavior. Since our definitions of all the order parameters include a normalization by a factor of L^3 to render them intensive, $\langle \mathcal{O}^2 \rangle$ is expected to vanish as L^{-3} in a phase with no such ordering tendency at all, but tend to a finite nonzero value in the thermodynamic limit in the presence of long-range order.

The one exception to this is $\langle \omega^2 \rangle$, which is expected to have a somewhat different fall off in phases without sublattice order: If the phase breaks lattice translation symmetry along two Cartesian axes and has columnar order, then one expects a $1/L^3$ fall off, but a layered phase (which breaks lattice translation symmetry in only one direction) is expected to display a $1/L^6$ fall off of $\langle \omega^2 \rangle$. As we will see below, the layered phase

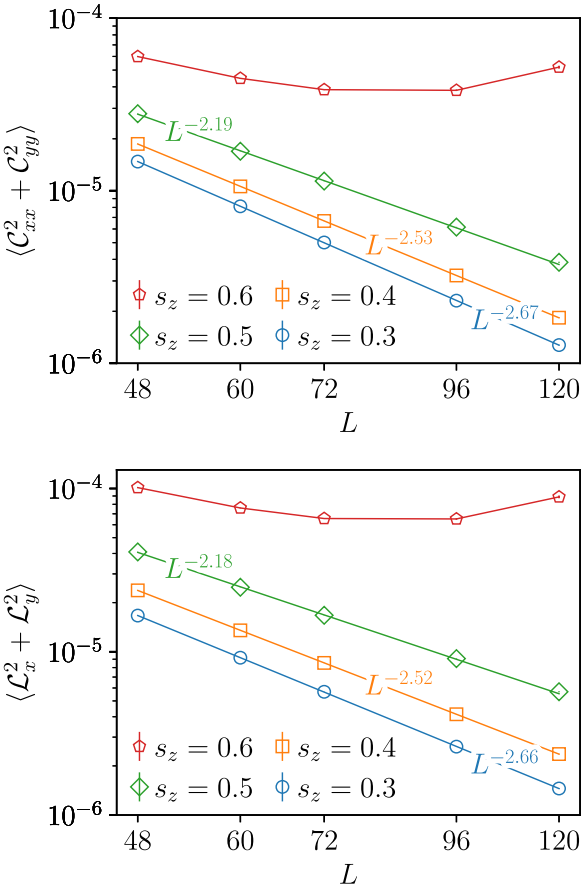

FIG. 6. $\langle \mathcal{C}_{xx}^2 + \mathcal{C}_{yy}^2 \rangle$ (top) and $\langle \mathcal{L}_x^2 + \mathcal{L}_y^2 \rangle$ (bottom) as a function of the system size L for $s_z \in [0.3, 0.6]$ along the $e = 0$ cut (dashed line in Fig. 2) that crosses the phase boundary between the z-layered phase and the sublattice-ordered phase. Both axes are plotted on a logarithmic scale. At $s_z = 0.3$, 0.4, and 0.5 the system is in the z-layered phase. Straight lines represent power-law fits of the form $c/L^{1+\eta_{3d}}$. In the layered phase, the best-fit values are in the range $1 < \eta_{3d} < 2$. This unambiguously signals the presence of three-dimensional power-law correlations of the corresponding transverse symmetry breaking order parameters, although there is true long-range order only in the z-layering order parameter (as already suggested by the data in Fig. 3). At $s_z = 0.6$, both quantities appear to extrapolate to a nonzero value in the large-L limit, indicating that translation symmetry is broken in all three Cartesian directions. See Secs. II and IV for details.

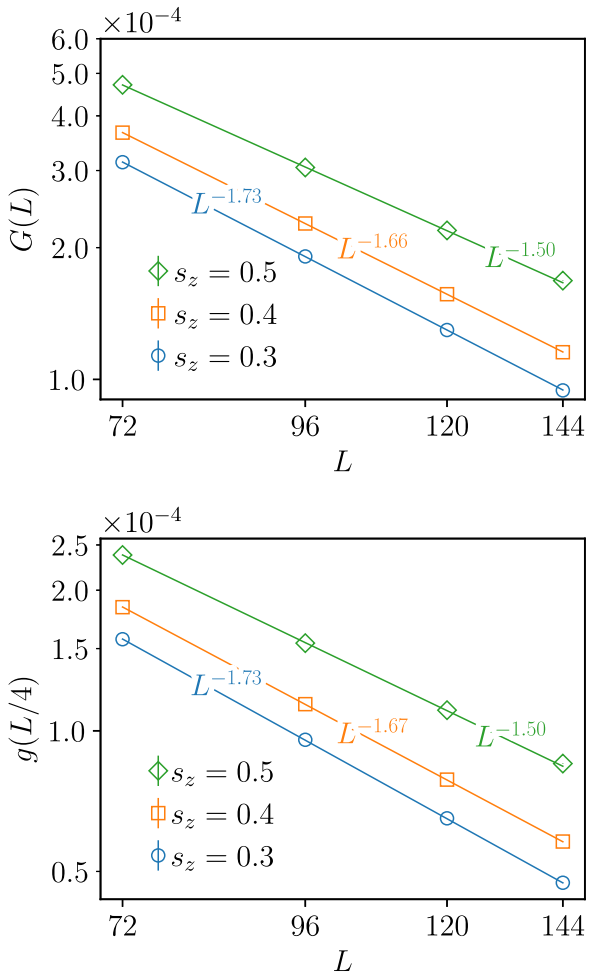

FIG. 7. $G(L)$ (top) and $g(L/4)$ (bottom) as a function of L on the $e = 0$ cut (dashed line in Fig. 2) for $s_z \in [0.3, 0.5]$. Both axes are plotted on a logarithmic scale. At $s_z = 0.3$, 0.4, and 0.5 the system is in the z-layered phase. Straight lines represent power-law fits of the form $c/L^{\eta_{2d}(0)}$. Since the best-fit values are in the range $1 < \eta_{2d}(0) < 2$, this provides an unambiguous signature of power-law intraslab correlations of the transverse symmetry-breaking order parameters in the layered phase. See Secs. II and IV for details.

that arises in our hard-plate system has power-law order in the transverse directions in addition to breaking lattice translation symmetry along the layering direction. As a result of this, we expect $\langle \omega^2 \rangle$ to display a power-law fall off with an exponent somewhat smaller than 6.

In a phase with three-dimensional power-law order, we expect the mean-square order parameter $\langle \mathcal{O}^2 \rangle$ to vanish as $L^{-(d-2+\eta_{3d})}$ whenever the correlation function of the corresponding order parameter density falls off as $1/r^{d-2+\eta_{3d}}$ with $\eta_{3d} < 2$ ($d = 3$ here). Note that $\langle \mathcal{O}^2 \rangle$ cannot distinguish between a disordered phase and a power-law-ordered phase with $\eta_{3d} > 2$, since $\langle \mathcal{O}^2 \rangle \sim 1/L^3$ in both cases; however, the two can still be distinguished by measuring the correlation function of the local order parameter density. Naturally, these expectations do not apply in the case of the sublattice order parameter ω, which is not the sum of a local order parameter density.

For each of these order parameters, we also monitor the Binder ratio $U_{\mathcal{O}^2}$:

$$U_{\mathcal{O}^2} = \frac{\langle \mathcal{O}^4 \rangle}{\langle \mathcal{O}^2 \rangle^2}. \tag{7}$$

In an ordered state, this ratio tends to unity in the thermodynamic limit. In a disordered state, it tends to a value larger than one, which depends on the number of independently fluctuating components that make up $\mathcal{O}$. Thus, the Binder ratio of a scalar order parameter tends to a limiting value of 3, while that of a two-component vector tends to 2, and so on.

To probe the nature of the z-layered phase in more detail, we also study the intraslab and interslab correlation functions of the transverse components of the layering order parameter.

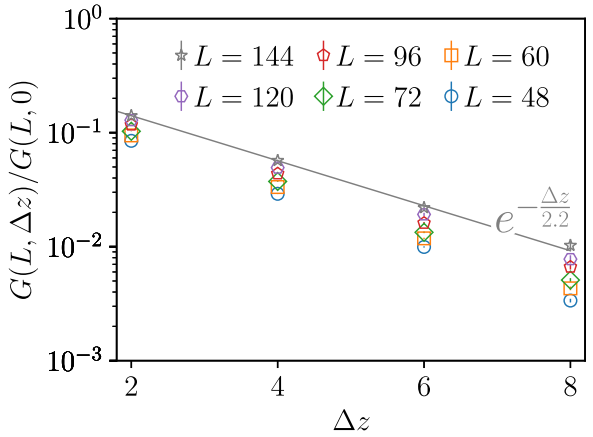

FIG. 8. The normalized interslab correlator $G(L, \Delta z)/G(L, 0)$ of the transverse components of the layering order parameter (integrated over each slab) at $e = 0$ and $s_z = 0.4$ at each fixed size L plotted against the interslab distance Δz. The data at each fixed L fits well to an exponentially decaying form. The corresponding exponential fit is shown explicitly for one value of L (note that the y axis is on a logarithmic scale). But data at a fixed nonzero Δz do not appear to converge to a limiting thermodynamic value even at the largest size L accessible to our numerics. This is explored further in Fig. 9. See Secs. II and IV for details.

To this end, we first define

$$l_{x\perp}(z) = \frac{1}{L^2}\sum_{x,y} l_x(x, y, z),$$
$$l_{y\perp}(z) = \frac{1}{L^2}\sum_{x,y} l_y(x, y, z). \tag{8}$$

In terms of $l_{x\perp}$ and $l_{y\perp}$, we can now define

$$G(L, \Delta z) = \frac{1}{L}\sum_z \langle (l_{x\perp}(z) l_{x\perp}(z + \Delta z) + l_{y\perp}(z) l_{y\perp}(z + \Delta z)\rangle. \tag{9}$$

In what follows, we will use $G(L)$ as shorthand for $G(L, \Delta z = 0)$, while retaining the second argument when Δz is nonzero. In principle, the sum over z in the definition of $G(L, \Delta z)$ should be taken only over "occupied" slabs, with the convention that all z plates are assigned to the occupied slabs. However, we have checked that summing over all z, which is computationally simpler, gives qualitatively similar results. This motivates the definition above.

As an independent check on this way of looking at the intraslab correlations, we have also measured the r dependence of $g(r, \Delta z = 0)$, defined as the connected intraslab correlation function of l_x and l_y within a single slab at a transverse distance of r. Power-law columnar order within each occupied slab, with intraslab correlator scaling as $g(r, \Delta z = 0) \sim 1/r^{\eta_{2d}(0)}$, is expected to correspond to $G(L) \equiv G(L, \Delta z = 0) \sim 1/L^{\eta_{2d}(0)}$ if $\eta_{2d}(0) < 2$, and $G(L) \sim 1/L^2$ if $\eta_{2d}(0) > 2$. As we show below, our results are consistent with this expectation. Similarly, when the correlations of l_x and l_y at a fixed nonzero Δz decay as $g(r, \Delta z) \sim 1/r^{\eta_{2d}(\Delta z)}$ with transverse distance r, we expect $G(L, \Delta z) \sim 1/L^{\eta_{2d}(\Delta z)}$ if $\eta_{2d}(\Delta z) < 2$, and a measured $G(L, \Delta z) \sim 1/L^2$ if $\eta_{2d}(\Delta z) > 2$.

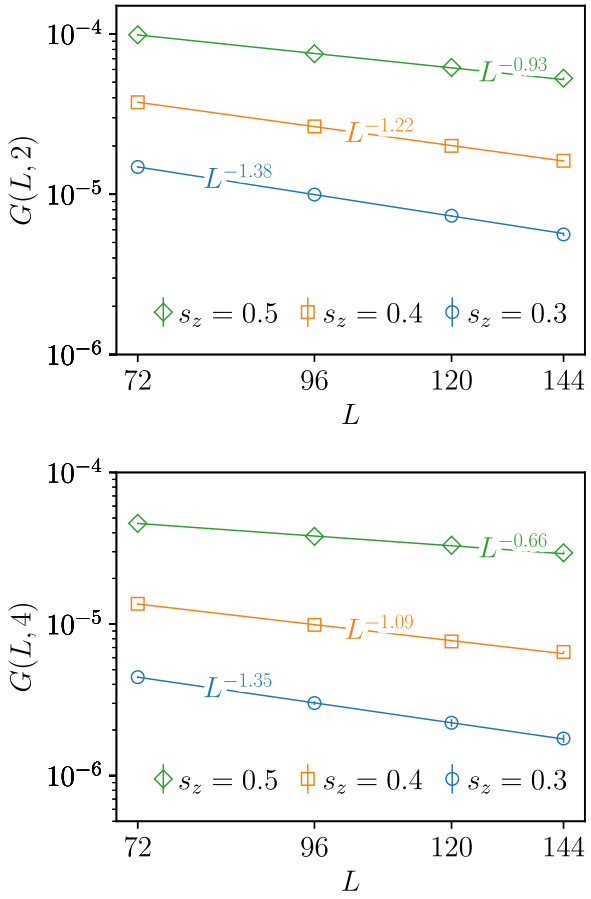

FIG. 9. The interslab correlators $G(L, 2)$ (top) and $G(L, 4)$ (bottom) of the transverse components of the layering order parameter (integrated over each slab) as a function of the system size L on the $e = 0$ cut (dashed line in Fig. 2) for $s_z \in [0.3, 0.5]$. Both axes are plotted on a logarithmic scale. At $s_z = 0.3, 0.4$, and 0.5, the system is in the z-layered phase. Straight lines represent power-law fits of the form $1/L^{\eta_{2d}(2)}$ (top) and $1/L^{\eta_{2d}(4)}$ (bottom). This is the origin of the L-dependent drift seen in Fig. 8. See Secs. II and IV for details.

With this background, we now present some representative results of such a study, focusing on the two cuts through the phase diagram displayed in Fig. 2.

A. $e = 0$

Along the $e = 0$ cut, we have $s_x = s_y = (3 - s_z)/2$. The data shown earlier in Fig. 3 strongly suggests that the system is in a layered phase for small s_z and a sublattice-ordered state near $s_z = 1$. Figure 6 shows the L dependence of the transverse columnar order parameter $\langle \mathcal{C}_{xx}^2 + \mathcal{C}_{yy}^2 \rangle$ and the transverse layering order parameter $\langle \mathcal{L}_x^2 + \mathcal{L}_y^2 \rangle$ for various s_z in the vicinity of the transition from the z-layered phase to the sublattice-ordered phase. Note that both these order parameters behave in the same way, although one of them uses the double-plate definition of the columnar vector and the other relies on the single-plate definition of the layering vector. At $s_z = 0.3, 0.4$, and 0.5, we see that both these order parameters go to zero with increasing L, confirming that translational symmetry is only broken in the z direction. At $s_z = 0.6$, however, both these order parameters appear to extrapolate to a

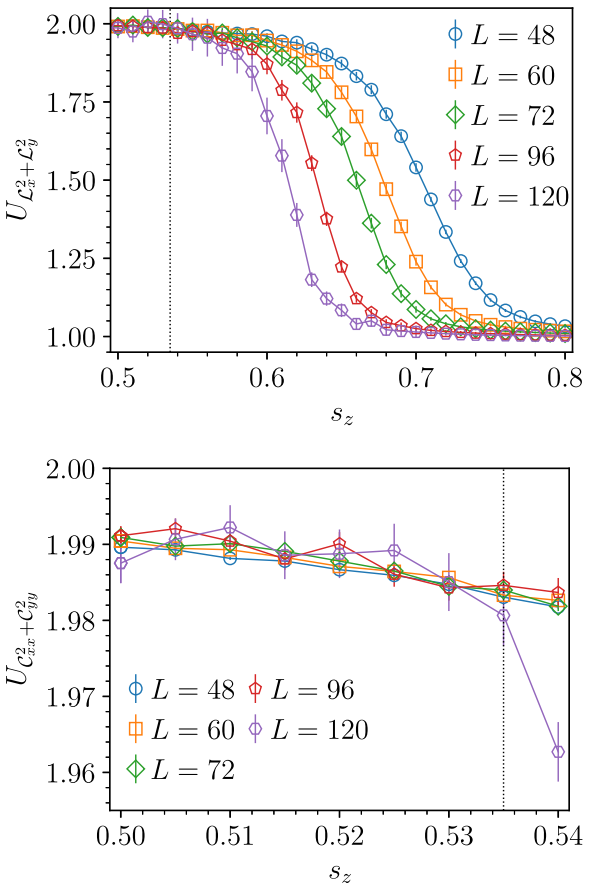

FIG. 10. The Binder ratios $U_{\mathcal{L}_x^2+\mathcal{L}_y^2}$ (top) and $U_{\mathcal{C}_{xx}^2+\mathcal{C}_{yy}^2}$ (bottom) plotted as a function of the system size L on the $e = 0$ cut (dashed line in Fig. 2) across the transition from the z-layered phase to the sublattice-ordered phase for $s_z \in [0.5, 0.8]$ (top) and in a zoomed-in region for $s_z \in [0.5, 0.54]$ (bottom). Curves for various L appear to stick together for $s_z \lesssim 0.535$, and splay away from each other above this threshold. This threshold is identified with the phase transition along the $e = 0$ cut. The dotted vertical lines (top and bottom) are at $s_z = 0.535$. The data for the bottom plot has been obtained by averaging over a larger number of seeds to reduce the error bars. See Secs. II and IV for details.

nonzero value in the large-L limit, signaling that symmetry is broken in all three directions, as expected in the sublattice-ordered state.

The L dependence of these transverse order parameters also provides evidence for an interesting aspect of the z-layered phase, namely, the presence of power-law order in the transverse directions. In Fig. 6, this is inferred from the power-law falloff $\propto 1/L^{1+\eta_{3d}}$ of these quantities at large L. The best-fit value of η_{3d} is in the range $1 < \eta_{3d} < 2$ and varies smoothly with s_z. To explore this further, we have also studied the transverse order *within* each occupied slab by measuring $G(L, \Delta z = 0)$ [Eq. (9)] as well as the corresponding connected correlation function $g(r, \Delta z = 0)$ evaluated at $r = L/4$. From Fig. 7, we see that both of these decay with L as a power-law $\sim 1/L^{\eta_{2d}(0)}$. In the layered phase, the two-dimensional exponent $\eta_{2d}(0)$ is seen to vary smoothly with s_z in the range $1 < \eta_{2d}(0) < 2$. These transverse power-law correlations point to the unusual and interesting nature of this layered phase, which is discussed in more detail in Sec. V.

If the transverse components of the layering vectors within different occupied slabs separated by Δz along the z axis had only been coupled to each other via weak correlations decaying exponentially with increasing Δz, then the measured η_{3d} would have satisfied the equality $\eta_{3d} = 1 + \eta_{2d}(0)$. However, we find that the measured η_{3d} and $\eta_{2d}(0)$ always satisfy $\eta_{3d} < 1 + \eta_{2d}(0)$. To explore this further, we have also measured $G(L, \Delta z)$ for various Δz and L in the layered phase. As shown in Fig. 8, the normalized interslab correlator $G(L, \Delta z)/G(L, 0)$ at $s_z = 0.4$ does indeed appear to fall off exponentially with Δz at fixed L. However, at fixed nonzero Δz, data for different L do not appear to converge to a limiting value even at the largest L accessible to our numerical study.

To understand this drift better, we study the L dependence of $G(L, \Delta z)$ for $\Delta z = 2, 4$ at various s_z in the layered phase. This is shown in Fig. 9. We find that $G(L, \Delta z)$ decays as a power law with increasing L for fixed Δz. The corresponding exponent $\eta_{2d}(\Delta z)$ *depends on* Δz in addition to its dependence on the fugacity s_z. Indeed, it appears to *decrease* with increasing Δz. This is the underlying reason for the drift seen earlier (Fig. 8) in $G(L, \Delta z)/G(L, 0)$.

Thus, as we increase s_z, the system initially remains in a z-layered phase with power-law correlations of the transverse components of the layering and columnar vectors. Beyond a threshold value, translational symmetry is broken in all three directions and there is a transition to a sublattice-ordered state. To locate this transition, we monitor the s_z and L dependence of Binder ratios of the transverse order parameters. A second order critical point between a conventional z-layered phase (with no power-law transverse order) and the sublattice-ordered phase is expected to give rise to a crossing of the Binder ratio curves corresponding to different sizes L, whereas a first order transition between two such phases is expected to lead to nonmonotonic behavior of these curves near the transition.

However, we see neither of these behaviors. Instead, we see in Fig. 10 that the Binder ratios for different L seem to stick together for $s_z \lesssim 0.535$, and splay apart for $s_z \gtrsim 0.535$. This sticking of the transverse Binder ratio curves corresponding to different L is what one expects in a phase with power-law correlations of the transverse order parameters. Indeed, the stick and splay behavior of the Binder ratios in Fig. 10 is reminiscent of similar behavior of the Binder ratio of the columnar order parameter in the vicinity of the transition between long-range columnar order and power-law columnar order in the two-dimensional fully packed lattice gas of hard squares and dimers [18]. Thus, from the data shown in this figure, we estimate that the transition from the z-layered phase to the sublattice-ordered phase occurs at $s_z \approx 0.535$ on the $e = 0$ cut.

It is important to emphasize that the behavior of the layering and columnar order parameters at the isotropic point ($s_z = 1$, $e = 0$) does not by itself provide unambiguous evidence of sublattice ordering. This is because an ergodic Monte Carlo simulation that can access all the symmetry related ordered configurations of a columnar or layered state at the isotropic point would also lead to nonzero values in the thermodynamic limit for all three components of the layering and columnar vectors. To obtain a direct confirmation of the sublattice-ordered nature of the phase, we have therefore studied the L

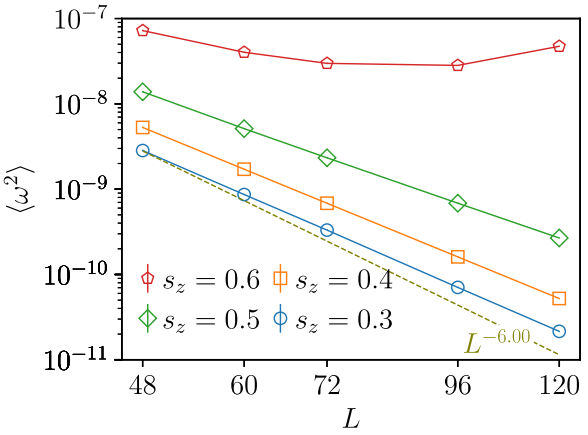

FIG. 11. $\langle\omega^2\rangle$ for $s_z \in [0.3, 0.6]$ as a function of the system size L along the $e = 0$ cut across the transition from the z-layered phase to the sublattice-ordered phase. The x and y axes are plotted on a logarithmic scale. At $s_z = 0.3, 0.4$, and 0.5 the system is in the z -layered phase. In this regime, $\langle\omega^2\rangle$ falls off with L in a power-law manner, but somewhat slower than c/L^6 (dashed straight line) due to the presence of power-law correlations of the transverse layering order parameters within the occupied slabs. At $s_z = 0.6$, $\langle\omega^2\rangle$ appears to extrapolate to a nonzero value in the large-L limit, signaling the presence of sublattice order. See Secs. II and IV for details.

dependence of $\langle\omega^2\rangle$. In Fig. 11, we display this L dependence for a few values of s_z on either side of the threshold identified in Fig. 10. From this data, we see that $\langle\omega^2\rangle$ decays to zero as a power-law $\propto 1/L^p$ at large L with $p < 6$ in the layered phase, but appears to extrapolate to a nonzero value in the large L limit for $s_z = 0.6$. This establishes that the phase in the vicinity of the isotropic point has sublattice order. It is also consistent with the fact that the layered phase has power-law transverse correlations which cause $\langle\omega^2\rangle$ to fall off with increasing size slower than $\sim 1/L^6$.

As s_z is increased further along the $e = 0$ cut, the sublattice-ordered phase terminates in a transition to a z columnar-ordered phase, which breaks lattice translation symmetry in the x and y directions, but has full lattice translation symmetry in the z direction. This can be seen from the s_z dependence of the Binder ratios of the relevant order parameter $\langle\mathcal{L}_z^2\rangle$ for various values of L. This is shown in the top panel of Fig. 12, from which one sees that the Binder ratios cross at a critical fugacity $s_z \approx 1.095$. Since the Z_2 symmetry of lattice translations in the z direction is restored upon crossing this transition, while translation symmetry in other directions remains broken on either side of the transition, one expects this transition to be in the three-dimensional Ising universality class.

To confirm this expectation, we use the known correlation length exponent [27] $\nu \approx 0.63$ for the Ising universality class in three dimensions and attempt a collapse of the Binder ratio data in the vicinity of this crossing point. This is shown in the middle panel of Fig. 12. In addition, we check if $\langle\mathcal{L}_z^2\rangle$, when rescaled by a factor of $L^{1+\eta_{\text{crit.}}}$ (using the three-dimensional Ising value $\eta_{\text{crit}} \approx 0.0363$ [27] of the anomalous exponent) shows a similar crossing at the critical fugacity $s_z \approx 1.095$. This is shown in the bottom panel of Fig. 12. Our conclusion,

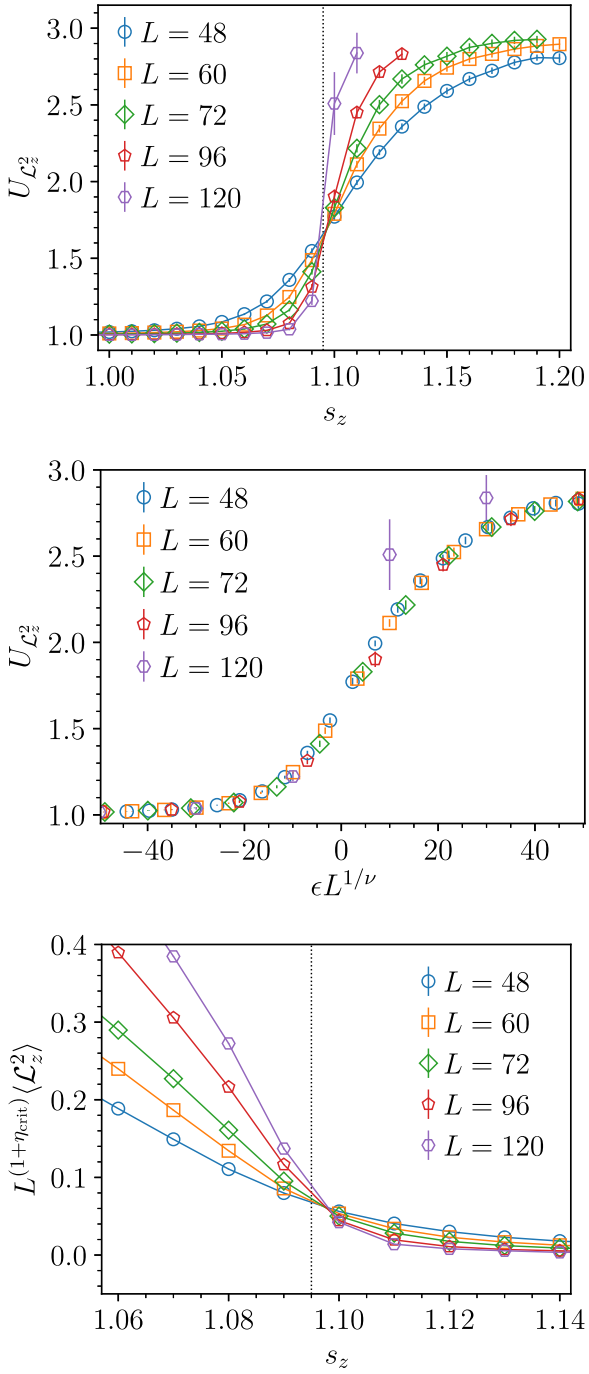

FIG. 12. (top) $U_{\mathcal{L}_z^2}$ as a function of s_z on the $e = 0$ cut (dashed line in Fig. 2) for $s_z \in [1, 1.2]$ across the sublattice-ordered to z columnar-ordered transition. The Binder ratio curves for various L cross at $s_z \approx 1.095$ giving us an estimate of the critical fugacity. (middle) Scaling collapse of $U_{\mathcal{L}_z^2}$ as a function of $\epsilon L^{1/\nu}$ with $\epsilon = (s_z - 1.095)$ and $\nu = 0.63$. (bottom) $\langle\mathcal{L}_z^2\rangle$ is rescaled by a factor of $L^{1+\eta_{\text{crit.}}}$ (with $\eta_{\text{crit.}} = 0.0363$) and plotted as a function of s_z. Curves corresponding to different L are seen to cross close to $s_z \approx 1.095$, consistent with the crossing seen in the Binder ratio curves. The dotted vertical lines (top and bottom) are at $s_z = 1.095$. Values of ν and $\eta_{\text{crit.}}$ correspond to the three-dimensional Ising universality class [27]. See Secs. II and IV for details.

based on the data displayed in these figures, is that the transition is indeed in the Ising universality class.

In summary, along the $e = 0$ cut shown in Fig. 2, the system is in a z-layered phase with power-law transverse correlations for $0 \leqslant s_z \lesssim 0.535$, undergoes a transition at $s_z \approx 0.535$ to a sublattice-ordered phase, remains in this sublattice-ordered phase for $0.535 \lesssim s_z \lesssim 1.095$, undergoes a transition to a z columnar-ordered phase at $s_z \approx 1.095$, and remains columnar-ordered beyond this as s_z approaches the $s_z = 3$ corner of the fugacity triangle. The universality class of the first transition, from layered to sublattice-ordered, has not been determined in our work. The second transition has properties consistent with expectations for a three-dimensional Ising transition. The schematic phase diagram shown in Fig. 2 was drawn using this information along with inputs from the other scan (discussed next) along the $e = 0.3$ cut through the fugacity triangle.

B. $e = 0.3$

Along the $e = 0.3$ cut, we have $s_x = s_y + 0.3$, $s_y = (2.7 - s_z)/2$. The data (shown in Fig. 3) for the various components of the layering order parameter strongly suggests that the system goes through a sequence of four phases as s_z is increased along this cut from $s_z = 0$ to $s_z = 2.7$. In order of increasing s_z these are the z-layered phase, the x columnar-ordered phase, the sublattice-ordered phase, the z columnar-ordered phase, and finally, the y-layered phase. This can be confirmed by a detailed analysis of the L dependence of the corresponding order parameters and Binder ratios, as we describe below.

Figure 13 shows the L dependence of the x component of the columnar order parameter $\langle \mathcal{C}_x^2 \rangle$ and the y component of the layering order parameter $\langle \mathcal{L}_y^2 \rangle$ for various s_z in the vicinity of the transition from the z-layered phase to the x columnar-ordered phase. Note that we are now displaying our data for the single-plate definition of the columnar order parameter (unlike the analogous data displayed along the $e = 0$ cut). At $s_z = 0.3, 0.4$, and 0.5, we see that both these order parameters go to zero, confirming that translational symmetry is only broken in the z direction. At $s_z = 0.6$, however, both these order parameters appear to extrapolate to a nonzero value in the large-L limit, establishing that symmetry is broken in the y direction in addition to the z direction, as expected in the x columnar-ordered state.

In the z-layered phase, we see that $\langle \mathcal{C}_x^2 \rangle$ and $\langle \mathcal{L}_y^2 \rangle$ go to zero with increasing L in a power-law manner. The values of the exponent η_{3d} that describes this power-law behavior are somewhat different from the corresponding values along the $e = 0$ cut at the same values of s_z. This is not unexpected, since the strength of the power-law correlations in the transverse direction can of course depend on the value of e.

A more precise estimate of the critical value of s_z for the transition from the z-layered phase to the x columnar-ordered state can be obtained from the stick and splay behavior of the appropriate Binder ratios as in the $e = 0$ case. The Binder ratios corresponding to both the order parameters splay for $s_z \gtrsim 0.56$ as shown in Fig. 14, giving us an estimate of the critical fugacity associated with this transition.

As s_z is increased further along this $e = 0.3$ cut, the system transitions from the x columnar-ordered phase to the sublattice-ordered phase at $s_z \approx 1.065$. One expects this transition to be in the three-dimensional Ising universality class since the two phases differ only by the Z_2 symmetry breaking of lattice translations in the x direction. Our results (which are not displayed here to avoid repetition) are indeed consistent with this expectation, and our analysis of this transition is entirely analogous to our earlier analysis of the transition between the z columnar-ordered phase and the sublattice-ordered phase along the $e = 0$ cut.

When we move further along the $e = 0.3$ cut, we find that the sublattice-ordered phase terminates in a transition to the z columnar-ordered phase at $s_z \approx 1.125$. We determine the location of the transition point and analyze the scaling behavior in its vicinity in a manner entirely analogous to our study of the sublattice-ordered to z columnar transition on the

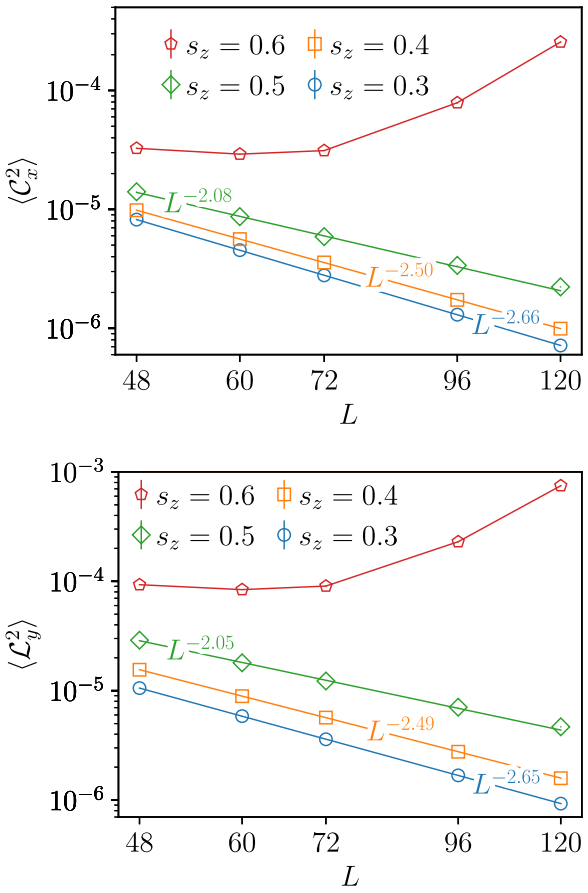

FIG. 13. $\langle \mathcal{C}_x^2 \rangle$ (top) and $\langle \mathcal{L}_y^2 \rangle$ (bottom) as a function of the system size L on the $e = 0.3$ cut (dotted line in Fig. 2) across the z layered to x columnar-ordered transition for $s_z \in [0.3, 0.6]$. In both top and bottom panels, both axes are plotted on a logarithmic scale. At $s_z = 0.3, 0.4$, and 0.5 the system is in the z-layered phase and $\langle \mathcal{C}_x^2 \rangle$ (top) and $\langle \mathcal{L}_y^2 \rangle$ (bottom) decay to zero in a power-law manner with increasing L. Straight lines represent power-law fits of the form $C/L^{1+\eta_{3d}}$, with $1 < \eta_{3d} < 2$. This is a clear signature of power-law correlations of the corresponding components of the columnar and layering order parameter densities. Note that the values of η_{3d} for these two order parameters are very close to each other for a given s_z but show clear variation with s_z in this regime. At $s_z = 0.6$, the system is in the x columnar-ordered phase and both these quantities appear to extrapolate to a nonzero value in the thermodynamic limit. See Secs. II and IV for details.

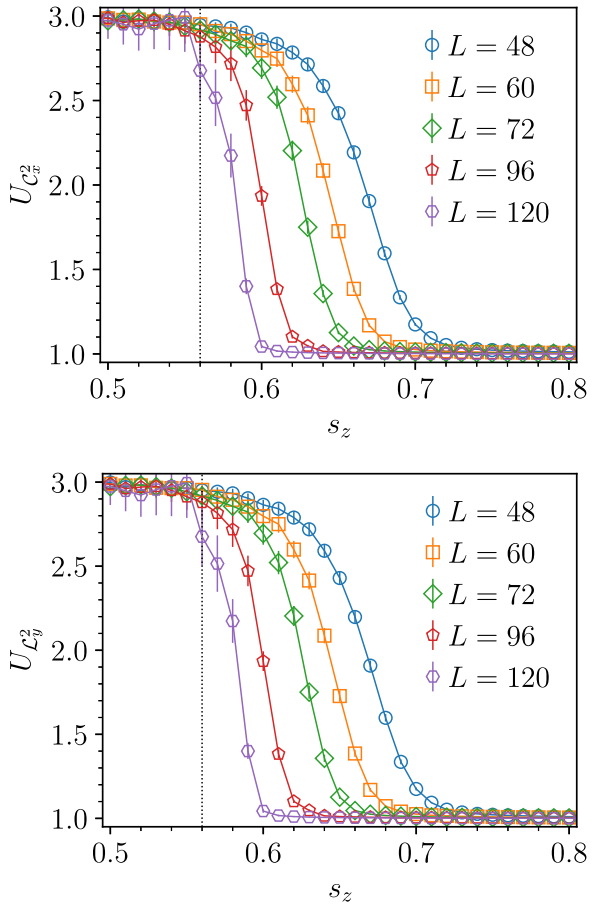

FIG. 14. The Binder ratios $U_{\mathcal{L}_x^2}$ (top) and $U_{\mathcal{L}_y^2}$ (bottom) as a function of s_z on the $e = 0.3$ cut (dotted line in Fig. 2) across the z layered to x columnar-ordered transition for $s_z \in [0.5, 0.8]$. Curves corresponding to different L stick to each other for $s_z \lesssim 0.56$ in the z-layered phase. For $s_z \gtrsim 0.56$, curves corresponding to different L start splaying apart, giving us an estimate of the critical fugacity for the z layered to x columnar-ordered phase transition on the $e = 0.3$ cut. The dotted vertical lines (top and bottom) are at $s_z = 0.56$. See Secs. II and IV for details.

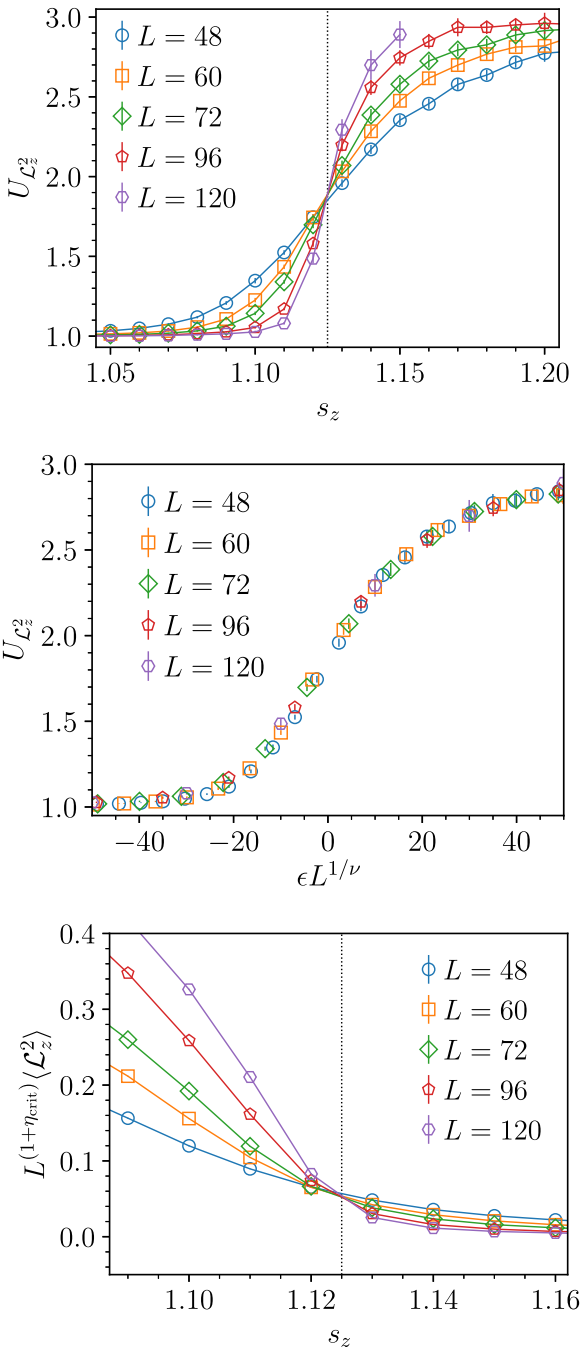

FIG. 15. (top) $U_{\mathcal{L}_z^2}$ as a function of s_z on the $e = 0.3$ cut (dotted line in Fig. 2) for $s_z \in [1.08, 1.16]$ across the sublattice-ordered to z columnar-ordered transition. The Binder ratio curves for various L cross at $s_z \approx 1.125$ giving us an estimate of the critical fugacity. (middle) Scaling collapse of $U_{\mathcal{L}_z^2}$ as a function of $\epsilon L^{1/\nu}$ with $\epsilon = (s_z - 1.125)$ and $\nu = 0.63$. (bottom) $\langle\mathcal{L}_z^2\rangle$ is rescaled by a factor of $L^{1+\eta_{\rm crit.}}$ (with $\eta_{\rm crit.} = 0.0363$) and plotted as a function of s_z. Curves corresponding to different L are seen to cross close to $s_z \approx 1.125$, consistent with the crossing seen in the Binder ratio curves. The dotted vertical lines (top and bottom) are at $s_z = 1.125$. Values of ν and $\eta_{\rm crit.}$ correspond to the three-dimensional Ising universality class [27]. See Secs. II and IV for details.

$e = 0$ cut in the previous subsection. This is shown in Fig. 15, where we see that our results are consistent with the behavior expected of the three-dimensional Ising universality class.

For even larger values of s_z the system undergoes yet another transition, from the z columnar-ordered phase to a y-layered phase. We omit a detailed study of this transition since the physics is entirely analogous to the previously presented results for the first transition between the z-layered phase and the x columnar-ordered phase along the $e = 0.3$ cut. A rough estimate of the critical fugacity of this transition can be obtained by looking at the value of s_z at which $\langle\mathcal{L}_x^2\rangle$ goes to zero in Fig. 3. It is $s_z \approx 1.55$.

In summary, along the $e = 0.3$ cut shown in Fig. 2, the system is in a z-layered phase for $0 \leqslant s_z \lesssim 0.56$ and undergoes a transition at $s_z \approx 0.56$ to an x columnar-ordered phase which persists in the range $0.560 \lesssim s_z \lesssim 1.065$. Next the system undergoes a transition at $s_z \approx 1.065$ to a sublattice-ordered phase which exists in the range $1.065 \lesssim s_z \lesssim 1.125$. Beyond $s_z \approx 1.125$, the system has z columnar order in the range $1.125 \lesssim s_z \lesssim 1.55$. Finally, the system undergoes a transition at $s_z \approx 1.55$ to a y-layered phase that is established beyond this threshold. The schematic phase diagram shown in Fig. 2 reflects these phases and phase boundaries.

Unlike for the Ising transitions between the sublattice-ordered phase and various columnar-ordered phases, we do not have a detailed understanding of the universality class of the transitions between the various layered phases and the sublattice-ordered phase, and between the various layered phases and columnar-ordered phases. This is because of the unusual nature of the layered phase, which displays power-law transverse ordering perpendicular to the layering direction.

What is the correct coarse-grained field-theoretical description of universal features of these continuous transitions? Although we are unable to answer this question, we note that the eventual answer would need to build on the answer to a related question: How can we understand the transverse power-law order of the layered phase itself within a coarse-grained effective field theory approach? Although our work does not fully answer this question either, the broad contours of an answer are sketched in Sec. V.

V. POWER LAWS IN THE LAYERED PHASE

Each occupied slab in the z-layered phase is power-law-ordered in the transverse directions, with power-law correlations of $\mathcal{L}_x$ and $\mathcal{L}_y$. To understand this better, we start in the $s_z \to 0$ limit. When $s_z = 0$, there are only x and y plates present, and these clearly organize themselves into occupied slabs separated from each other by one lattice spacing along the z axis. Viewed along the z axis, each such occupied slab is seen to be equivalent to a fully packed square lattice dimer model, with x plates represented by dimers along y links of the equivalent square lattice, and y plates represented by dimers along x links of this square lattice. The transverse power-law order of the occupied layers is simply understood in this limit as being a consequence of the power-law columnar order of the fully packed dimer model on the square lattice. Thus, at $s_z = 0$, we expect power-law columnar order with power-law exponent $\eta_{2d} = 2$.

As mentioned in Sec. I, the power-law correlations of the fully packed square lattice dimer model can be understood via a coarse-grained field theory whose action is written in terms of a fluctuating scalar height field that represents the electrostatic potential of a system of fluctuating dipoles:

$$S_{2d} = \pi g \int d^2 r (\nabla_\perp h)^2,$$
$$Z \propto \int \mathcal{D}h \exp(-S), \tag{10}$$

with $g = 1/2$. In this description the local density of x dimers (which represent y plates) is given by $(-1)^{x+y}\partial_y h + \mathcal{A}(-1)^x \cos(2\pi h)$, while the local density of y dimers (which represent x plates) is given by $(-1)^{x+y+1}\partial_x h + \mathcal{A}(-1)^y \sin(2\pi h)$.

When $s_z = \epsilon$, with $\epsilon > 0$ but very small, z plates are allowed. However, and this is key, the only configurations that contribute to the partition function in the thermodynamic limit have *pairs* of z plates, stacked one above the other in the z direction. When two such z plates are stacked one above the other in an occupied slab, they can be represented in the equivalent two dimensional system by a small admixture of hard squares introduced into the fully packed square lattice dimer model. The fugacity of these hard squares is of order ϵ^2. This small density of hard squares increases the stiffness of the fluctuating height field, so that $g(\epsilon) = 1/2 + \mathcal{O}(\epsilon^2)$, leading to a decrease in the value of η_{2d}, so that $\eta_{2d} = 2 - \mathcal{O}(\epsilon^2)$ [18].

If such a pair of z plates straddles two neighboring occupied slabs, then it can be replaced by a *pair* of parallel x or y plates that straddle the two occupied slabs. To $\mathcal{O}(\epsilon^2)$, these are the leading defects that destroy perfect layering and couple neighboring occupied slabs. Crucially, single x or y plates straddling neighboring occupied slabs do not contribute in the thermodynamic limit. Such plates can be viewed as a pair of holes in one layer of each of the two adjacent occupied slabs. The full-packing constraint ensures that this pair of holes, which is a dipolar defect from the point of view of the equivalent problem of hard squares and dimers, cannot move on its own. In effect, the full-packing constraint ensures that these dipolar defects come in nearest-neighbor pairs. Thus, dipolar defects are confined into quadrupoles. This is very different from the purely two-dimensional problem of hard-squares and dimers. The fact that each occupied layer is actually part of a fully three-dimensional system is therefore crucial for understanding the nature of the defects, although our description is in terms of an equivalent two dimensional system.

We now argue that this confinement of the dipolar defects into quadrupoles is the reason that the power-law correlations within each occupied slab survive the coupling between neighboring occupied slabs. To see this, represent each occupied slab in the small ϵ limit as a two-dimensional system of hard-squares and dimers. Ignoring the coupling between neighboring occupied slabs for the moment, this can be described by the effective action:

$$S_0 = \pi g \sum_z \int d^2 r (\nabla_\perp h_z)^2. \tag{11}$$

The quadrupolar defects that couple the neighboring occupied slabs can then be represented by attractive interactions between one pair of parallel dimers in a layer and another such pair in the neighboring layer. This leads to terms in the effective action that couple the height fields of neighboring slabs:

$$S = S_0 + S_1 + S_2,$$
$$S_1 = \lambda \sum_z \int d^2 r \left[\left(\partial_x^2 h_z\right)\left(\partial_x^2 h_{z+1}\right) + \left(\partial_y^2 h_z\right)\left(\partial_y^2 h_{z+1}\right) \right]$$
$$+ \lambda' \sum_z \int d^2 r \left(\partial_{xy}^2 h_z\right)\left(\partial_{xy}^2 h_{z+1}\right),$$
$$S_2 = \lambda'' \sum_z \int d^2 r \cos\{4\pi [h_z(r) - h_{z+1}(r)]\}, \tag{12}$$

with λ, λ', and λ'' all vanishing in the $\epsilon \to 0$ limit. Along the renormalization group (RG) fixed line with action S_0 parameterized by g, all three perturbations that constitute S_1 and S_2 are seen to be *irrelevant* so long as $8/g > 4$, i.e., $g < 2$. The quadrupolar nature of the defects coupling neighboring power-law-correlated slabs is now seen to be the key reason for the stability of these power-law-correlated slabs at nonzero s_z: In the absence of the constraints that force the dipolar defects to be confined into quadrupoles, a cosine term of

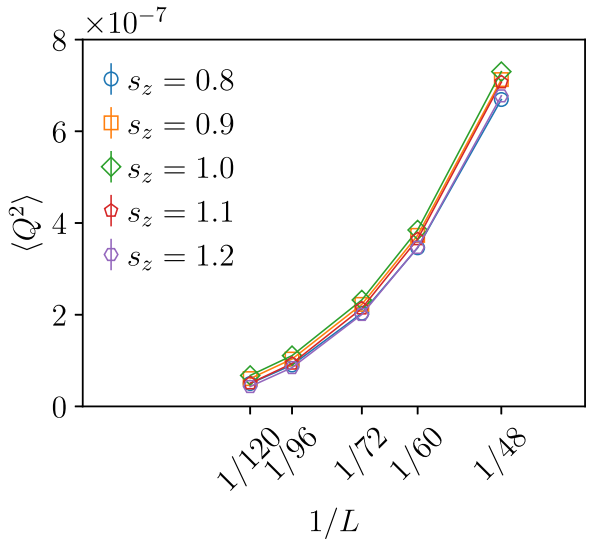

FIG. 16. The mean-square scalar sublattice order parameter $\langle Q^2 \rangle$ on the $e = 0$ cut (dashed line in Fig. 2) plotted as a function of the inverse system size $1/L$ for $s_z \in [0.8, 1.2]$, with a logarithmic scale for the $1/L$ axis. From the displayed data, we see that $\langle Q^2 \rangle$ decreases to a very small value at the largest size studied, and appears to extrapolate to zero in the thermodynamic limit. This behavior persists even in the sublattice-ordered phase. On the $e = 0$ cut, the sublattice-ordered phase exists between $s_z \sim 0.535$ (Fig. 10) and $s_z \sim 1.095$ (Fig. 12). See Secs. II and VI for details.

the form $\cos\{2\pi[h_z(r) - h_z(r+1)]\}$, representing a *single* x or y plate straddling two neighboring occupied slabs, would have been allowed. This term is relevant unless $2/g > 4$, i.e., $g < 1/2$, which is never the case since $g = 1/2$ for $s_z = 0$, and a small $\mathcal{O}(\epsilon)$ value of s_z only *increases* the value g from $g = 1/2$ to $g = 1/2 + \mathcal{O}(\epsilon^2)$. Thus, the transverse power-law correlations in this layered phase are stabilized by constraints imposed by full-packing, which confine dipolar interslab defects into quadrupoles.

VI. OUTLOOK

We conclude by highlighting some unresolved questions that may be worth addressing in follow-up studies. The first question has to do with our choice of sublattice order parameter ω defined in Eq. (5). As we have already discussed in Sec. II, one might *a priori* expect that the order parameter Q defined in Eq. (6) provides a natural measure of sublattice order. However, our results indicate that $\langle Q^2 \rangle$ defined in this way goes to a very small number in the thermodynamic limit even in the sublattice-ordered phase, and cannot be used to draw any reliable conclusions. This is illustrated in Fig. 16. Why this is the case is not entirely clear. Since we have been able to use ω to unambiguously detect the presence of sublattice order independent of this behavior of Q, it does not affect our results. This curious behavior of Q is an interesting unsolved puzzle.

The second set of questions has to do with the coarse-grained description discussed in Sec. V, which provides a natural explanation of the power-law correlations within each occupied slabs in the layered phase. It should be possible to develop this analysis further, to also describe the nature of the correlations between two different occupied slabs separated by a distance Δz in the layering direction. In particular, it would be interesting to develop a theory for the relationship between the intraslab power-law correlation exponent and the power-law exponent characterizing the L dependence of the three-dimensional transverse layering order parameter $\langle \mathcal{L}_x^2 + \mathcal{L}_y^2 \rangle$. Also worth pursuing is the effect of a small repulsive interaction between x and y plates in this layered phase with $s_z \ll s_x = s_y$. If this preserves the layered phase, then it would be interesting to explore its effects on the transverse columnar ordering.

Finally, we note that we have also explored in closely related work [23] a somewhat different layered phase, accessed by introducing vacancies into the isotropic fully packed system. Studying the effect of introducing a small density of vacancies in the layered phase ($s_z \ll s_x = s_y$) of the fully packed problem is a promising area for further study.

ACKNOWLEDGMENTS

We acknowledge useful discussions with R. Dandekar, R. Moessner, K. Ramola, and N. Shannon. G.R. gratefully acknowledges technical assistance from K. Ghadiali and A. Salve of the Department of Theoretical Physics (DTP) of the Tata Institute of Fundamental Research (TIFR), and from the Scientific Computing and Data Analysis section of the Okinawa Institute of Science and Technology (OIST). A portion of the results presented here was made possible by the generous allocation of computational resources made by DTP TIFR. The final stages of this work were facilitated by extensive computational resources provided by OIST. G.R. was supported by a graduate fellowship of the TIFR during a major part of this work and by the TQM unit at the Okinawa Institute of Science and Technology during the final stages of this work. The work of S.B. was supported by a postdoctoral fellowship of the DTP TIFR. D.M. was supported by a graduate fellowship of the Institute of Mathematical Sciences (IMSc). K.D. was supported at the TIFR by DAE, India and in part by a J. C. Bose Fellowship (No. JCB/2020/000047) of SERB, DST India, and by the Infosys-Chandrasekharan Random Geometry Center (TIFR). DD's work was partially supported by Grant No. DST-SR-S2/JCB-24/2005 of the Government of India, and partially by a Senior Scientist Fellowship of the National Academy of Sciences of India. G.R. performed the computational work with assistance from D.M. and wrote the first draft. K.D., R.R., and D.D. conceived the project, directed the computational work, and finalized the manuscript using inputs from all authors. S.B. performed exploratory simulations in the preliminary stages of the work.

[1] J. Villain, R. Bidaux, J. P. Carton, and R. Conte, Order as an effect of disorder, J. Phys. France **41**, 1263 (1980).

[2] C. L. Henley, The "Coulomb phase" in frustrated systems, Annu. Rev. Condens. Matter Phys. **1**, 179 (2010).

[3] R. W. Youngblood and J. D. Axe, Polarization fluctuations in ferroelectric models, Phys. Rev. B **23**, 232 (1981).
[4] R. Youngblood, J. D. Axe, and B. M. McCoy, Correlations in ice-rule ferroelectrics, Phys. Rev. B **21**, 5212 (1980).
[5] S. Papanikolaou, E. Luijten, and E. Fradkin, Quantum criticality, lines of fixed points, and phase separation in doped two-dimensional quantum dimer models, Phys. Rev. B **76**, 134514 (2007).
[6] F. Alet, Y. Ikhlef, J. L. Jacobsen, G. Misguich, and V. Pasquier, Classical dimers with aligning interactions on the square lattice, Phys. Rev. E **74**, 041124 (2006).
[7] P. Patil, I. Dasgupta, and K. Damle, Resonating valence-bond physics on the honeycomb lattice, Phys. Rev. B **90**, 245121 (2014).
[8] N. Desai, S. Pujari, and K. Damle, Bilayer coulomb phase of two-dimensional dimer models: Absence of power-law columnar order, Phys. Rev. E **103**, 042136 (2021).
[9] G. Rakala, K. Damle, and D. Dhar, Fractional Brownian motion of worms in worm algorithms for frustrated Ising magnets, Phys. Rev. E **103**, 062101 (2021).
[10] D. A. Huse, W. Krauth, R. Moessner, and S. L. Sondhi, Coulomb and Liquid Dimer Models in Three Dimensions, Phys. Rev. Lett. **91**, 167004 (2003).
[11] C. Xu and C. Wu, Resonating plaquette phases in SU(4) Heisenberg antiferromagnet, Phys. Rev. B **77**, 134449 (2008).
[12] A. F. Albuquerque and F. Alet, Critical correlations for short-range valence-bond wave functions on the square lattice, Phys. Rev. B **82**, 180408(R) (2010).
[13] Y. Tang, A. W. Sandvik, and C. L. Henley, Properties of resonating-valence-bond spin liquids and critical dimer models, Phys. Rev. B **84**, 174427 (2011).
[14] K. Damle, D. Dhar, and K. Ramola, Resonating Valence Bond wave Functions and Classical Interacting Dimer Models, Phys. Rev. Lett. **108**, 247216 (2012).
[15] S. Pankov, R. Moessner, and S. L. Sondhi, Resonating singlet valence plaquettes, Phys. Rev. B **76**, 104436 (2007).
[16] A. Vishwanath and D. Carpentier, Two-Dimensional Anisotropic Non-Fermi-Liquid Phase of Coupled Luttinger Liquids, Phys. Rev. Lett. **86**, 676 (2001).
[17] R. Mukhopadhyay, C. L. Kane, and T. C. Lubensky, Sliding Luttinger liquid phases, Phys. Rev. B **64**, 045120 (2001).
[18] K. Ramola, K. Damle, and D. Dhar, Columnar Order and Ashkin-Teller Criticality in Mixtures of Hard Squares and Dimers, Phys. Rev. Lett. **114**, 190601 (2015).
[19] C. Xu and M. P. A. Fisher, Bond algebraic liquid phase in strongly correlated multiflavor cold atom systems, Phys. Rev. B **75**, 104428 (2007).
[20] M. Pretko, Subdimensional particle structure of higher rank U(1) spin liquids, Phys. Rev. B **95**, 115139 (2017).
[21] Y. You, Z. Bi, and M. Pretko, Emergent fractons and algebraic quantum liquid from plaquette melting transitions, Phys. Rev. Res. **2**, 013162 (2020).
[22] Y. You and R. Moessner, Fractonic plaquette-dimer liquid beyond renormalization, Phys. Rev. B **106**, 115145 (2022).
[23] D. Mandal, G. Rakala, K. Damle, D. Dhar, and R. Rajesh, Phases of the hard-plate lattice gas on a three-dimensional cubic lattice, Phys. Rev. E **107**, 064136 (2023).
[24] O. F. Syljuåsen and A. W. Sandvik, Quantum Monte Carlo with directed loops, Phys. Rev. E **66**, 046701 (2002).
[25] W. Krauth and R. Moessner, Pocket Monte Carlo algorithm for classical doped dimer models, Phys. Rev. B **67**, 064503 (2003).
[26] C. Domb, M. S. Green, and J. L. Lebowitz, *Phase Transitions and Critical Phenomena*, Phase Transitions and Critical Phenomena No. 3 (Academic Press, San Diego, CA, 1972).
[27] A. Pelissetto and E. Vicari, Critical phenomena and renormalization-group theory, Phys. Rep. **368**, 549 (2002).